AIP | Physics of Plasmas

Conservation laws and conversion efficiency in ultraintense laser-overdense plasma interactions

M. C. Levy, S. C. Wilks, M. Tabak, and M. G. Baring

Citation: Phys. Plasmas **20**, 103101 (2013); doi: 10.1063/1.4821607
View online: http://dx.doi.org/10.1063/1.4821607
View Table of Contents: http://pop.aip.org/resource/1/PHPAEN/v20/i10
Published by the AIP Publishing LLC.

Conservation laws and conversion efficiency in ultraintense laser-overdense plasma interactions

M. C. Levy,[1,2,a)] S. C. Wilks,[2] M. Tabak,[2] and M. G. Baring[1]
[1]*Department of Physics and Astronomy, MS 108, Rice University, Houston, Texas 77005, USA*
[2]*Lawrence Livermore National Laboratory, Livermore, California 94551, USA*

(Received 21 June 2013; accepted 24 August 2013; published online 2 October 2013)

Particle coupling to the oscillatory and steady-state nonlinear force of an ultraintense laser is studied through analytic modeling and particle-in-cell simulations. The complex interplay between these absorption mechanisms—corresponding, respectively, to "hot" electrons and "hole punching" ions—is central to the viability of many ultraintense laser applications. Yet, analytic work to date has focused only on limiting cases of this key problem. In this paper, we develop a fully relativistic model in 1-D treating both modes of ponderomotive light absorption on equitable theoretical footing for the first time. Using this framework, analytic expressions for the conversion efficiencies into hole punching ions and into hot electrons are derived. Solutions for the relativistically correct hole punching velocity and the hot electron Lorentz factor are also calculated. Excellent agreement between analytic predictions and particle-in-cell simulations is demonstrated, and astrophysical analogies are highlighted. © *2013 AIP Publishing LLC*. [http://dx.doi.org/10.1063/1.4821607]

I. INTRODUCTION

The interaction of ultraintense laser light (normalized vector potential $a_0 = eE_L/(m_e c\omega_L) > 1$) with matter is characterized by the nonlinear action of the light.[1] The laser ponderomotive force f_L couples the incident photon flux into two primary kinetic modes: (1) "hole boring" or "hole punching" (hp) ions accelerated by the space-charge force associated with electrons under the excursion of time-averaged field energy gradients $\langle f_L \rangle \sim \nabla E_L^2$; and (2) relativistic "hot" electrons excited by the oscillatory component of f_L at $2\omega_L$. Optimizing the modes in which the photons are absorbed enables applications such as compact GeV-scale particle accelerators,[2] approaches to inertial confinement fusion[3] (ICF), and medical proton oncology.[4]

The complex interplay between the steady-state and oscillatory ponderomotive absorption processes is central to the viability of many ultraintense laser applications. Yet, to date, analytic models seeking to describe the interaction have only considered only limiting cases, e.g., assuming unitary coupling into either the steady-state hole punching (hp) absorption mode[1] or into the oscillatory mode.[5]

In this paper, we develop a fully relativistic 1-D analytic model treating both modes of ponderomotive light absorption on equitable theoretical footing for the first time. Using a kinematic framework, we derive analytic solutions for the (1) piston velocity u_p, (2) hole punching ion velocity u_i, (3) hot electron Lorentz factor γ_h, (4) conversion efficiency into hole punching ions f_a^p, and (5) conversion efficiency into hot electrons f_a^h. The model describes overdense plasma interactions and is insensitive to laser polarization assuming that bulk ions are swept up and fully reflected in the interaction. The general solutions are parameterized in terms of the total reflected light $\mathcal{R}$ and fundamental laser and plasma parameters. In specific limits, $\mathcal{R}$ is determined and the solutions recover well-established results from the literature. Excellent agreement between analytic predictions and particle-in-cell simulations is demonstrated.

The kinematic approach undertaken here considers the distribution functions f_s describing the exchange-mediating particles, i.e., those directly excited by the laser on the spatial scale c/ω_{pe} at the laser-plasma (LP) interface. The set s fully enumerates these populations, $s \in \{\text{hole punching ions, hole punching electrons, hot electrons}\}$; once the laser has coupled into these particles, energy and momentum may then cascade into other species in the plasma, e.g., drawing the return current[5] or generating positrons.[6] Now, in momentum space, $f_s = f_s(p^k; \langle p_s^0 \rangle)$ where $\langle p_s^0 \rangle = \int p^0 f_s dp^k$ (covariant notation is discussed in Sec. III). The task is thus to determine $\langle p_s^0 \rangle$ such that energy and momentum are conserved between the plasma and the laser driver.

This paper is structured as follows: Sec. II provides a brief review of existing analytic absorption models. In Sec. III, an overview of the approach undertaken here is discussed, and Secs. IV and V establish the foundations of the model. Section VI calculates the solutions for $\langle p_s^0 \rangle$, and Sec. VII derives the conversion efficiencies into hole punching ions and into hot electrons. In Sec. VII, the analytic results are compared to particle-in-cell simulations, and possible astrophysical applications are highlighted. Finally, concluding remarks are given in Sec. IX.

II. BACKGROUND

The task of understanding the critical interface exchange processes for $a_0 > 1$ LPI amounts to understanding the partitioning of the laser energy and momentum into hot electrons and hole punching ions. Yet, to date, a general framework treating both populations on equitable theoretical footing has

a)Electronic address: levy11@llnl.gov.

not been developed. The model of momentum conservation between an ultraintense laser and an overdense plasma was described by Wilks *et al.*,[1] which derived the hole punching velocity by balancing the laser momentum flux with that of the hole punching ions. Yet, in this model, the hot electrons were not accounted for, nor was energy conservation considered. Naumova *et al.*[7] extended this framework for relativistic hole punching ions and taking into account energy flux conservation.

This work considered full laser light reflection from the electron density peak bounding the radiation pressure-induced separation layer at the critical interface. In this context, the energy transferred to the plasma is that which is lost in the red-shifting of the reflected light, with an effective reflection coefficient[7] given by the relativistic doppler formula $\mathcal{R} = (1 - u_p/c)/(1 + u_p/c)$. This energy is assumed to be coupled with 100% efficiency into the punching ions. In the nonrelativistic limit, the energy absorbed by the ions is then simply $1 - \mathcal{R} \simeq 2u_p/c$, consistent with the simple estimate of Wilks and Kruer.[8] To the extent the laser piston structure is maintained with unit coupling into ions, recent measurements of the specular doppler shift[9] represent a 1: 1 measurement of the ion conversion efficiency.

In considering the fast electrons, Haines *et al.*[5] developed a "black box" model conserving both energy and momentum in the interaction, in a manner analogous to the Rankine-Hugoniot shock relations. Yet, this model took into account only the contributions from the hot electrons. More recently, Ping *et al.*[9] put forward a model that includes both the hot electron and hole punching ions; however, this model is constrained to the limit where the hole punching ions exchange momentum but not energy with the laser.

In the following sections, we present a novel analytic model extending this framework by allowing energetically significant absorption into both the steady-state and oscillatory modes for the first time. In Sec. VII, results from the model are compared to and shown to be in good agreement with particle-in-cell simulations.

III. COUPLING OF ULTRAINTENSE LASER LIGHT TO AN OVERDENSE PLASMA

We consider the *steady-state* laser-plasma interaction *at the coupling stage* in the *laboratory frame*. Consider the small volume at the laser-plasma interface comprising a few c/ω_{pe} in a axial extent, depicted schematically in Fig. 1. The laser is incident on the volume from the left and excites plasma particles which leave the volume on the right-hand side. All particles in the region are assumed to interact with the laser and may be accelerated relativistically by coupling into either the oscillatory or the steady-state absorption mode. The total electron density is n_e, which may take on any value that is relativistically opaque to the laser light.[10] Ions in the interface are assumed to have uniform charge state Z given by the quasi-neutrality condition, $n_i = n_e/Z$.

Absorption of ultraintense laser light by an overdense plasma amounts, in effect, to the coupling between an incident photon flux and particles comprising the moving plasma interface. It follows that we consider *only* plasma particles

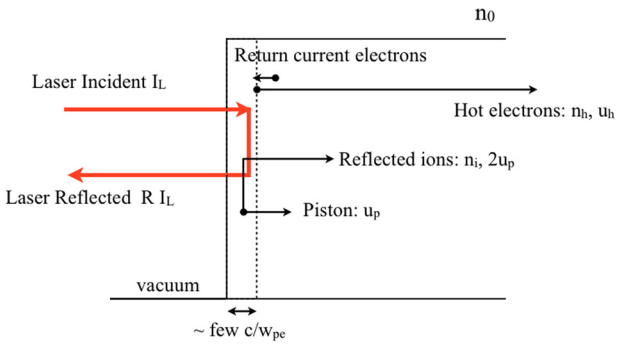

FIG. 1. Schematic depicting the laser plasma coupling in the interaction region with $n_0 = n_e = n_i/Z$ where Z is the ion charge state. The laser piston boundary is represented by the dashed line.

that mediate the energy and momentum exchange, i.e., those directly excited by the laser on the spatial scale c/ω_{pe} at the laser-plasma (LP) interface. The set s fully enumerates these populations,

$$s \in \{\text{hp ions, hp electrons, hot electrons}\}, \tag{1}$$

where in the following sections each species will be referred to by its numeric index. Once the laser has coupled into these populations, energy and momentum may then cascade into other species in the plasma. An important example of this is the collective plasma excitation of a return current in order to neutralize the fast electron current.[5]

The evolution of particle distribution functions $f_s(x^\mu, p^\mu)$ in Eq. (1) is determined by the Boltzmann-Vlasov equation,

$$\left(\frac{dx^\mu}{d\tau}\frac{\partial}{\partial x^\mu} + \frac{dp^k}{d\tau}\frac{\partial}{\partial p^k}\right) f_s = 0, \tag{2}$$

where τ is the proper time.[11,12] The Minkowski tensor $\eta^{\mu\nu}$ has signature (–, +, +, +); the greek sub- and super-scripts represent tensor indices $\mu \in \{0,1,2,3\}$; the latin indices $k \in \{1,2,3\}$ run over the spatial subset; the s subscript is reserved for particle species and for clarity will be distinguished from tensor indices where necessary. Collisional coupling is assumed to be negligible and the characteristics of Eq. (2) are given by,

$$\frac{dx^\mu}{d\tau} = \frac{p^\mu}{m_s}, \qquad \frac{dp^k}{d\tau} = -\frac{q_s}{m_s}F^{k\mu}p_\mu, \tag{3}$$

where the momentum characteristic includes spatial components due to the mass-shell restriction.[12] In Eqs. (2) and (3), q_s is the electric charge, m_s is the rest mass and $F^{\mu\nu}$ represents the field strength tensors.

The approach undertaken in this paper considers the parameters of f_s that satisfy conservation of energy and momentum between the ultraintense photon flux and relativistic particle fluxes excited in the plasma, e.g., moments of Eq. (2). In momentum space, $f_s = f_s(p^k; \langle p_s^0 \rangle)$ where $\langle p_s^0 \rangle = \int p^0 f_s dp^k$. We thus seek to determine $\langle p_s^0 \rangle$ for the hp particles and hot electrons.

For the former population, we note that the "laser piston"[7] is characterized by the strong electrostatic potential

generated by the steady-state component of the laser ponderomotive force,[13]

$$\mathbf{f_L} = \nabla\left(\frac{n_{cr}}{n_e}a_0^2\right)m_e c^2, \tag{4}$$

where n_e is the electron density in the laser-plasma interface. As the piston propagates into the target, we assume that background particles are swept up and fully reflected.[1,7,14,15] Electrons reflect from the piston head, while ions are pulled in by the potential and reflect from ions bounding the piston on the downstream side. Electrons and ions are both reflected at the same velocity, u_i. As such, we assume they are adequately represented in momentum space as distribution functions of the same form,

$$f_{s_n}(\beta) = \frac{C_n n_n}{\sqrt{2\pi\Theta_n}\gamma_i^{3/2}} e^{-\frac{(\gamma\beta-\gamma_i\beta_i)^2}{2\gamma_i^2\Theta_n}}, \quad n \in \{1,2\}, \tag{5}$$

where, related to Eq. (1), f_{s_1} represents the hole punching ion distribution and f_{s_2} represents the hole punching electron distribution. m_n is the mass, n_n is the reflected particle density, C_n is a normalization constant and $\Theta_n = T_n/(m_n c^2)$ where T_n is the temperature of population s_n. $\beta = u/c$ for the particle velocity u and $\beta_i = u_i/c$ for the reflected particle velocity u_i, with the Lorentz factors defined in the usual manner, $\gamma = (1-\beta^2)^{-1/2}$. Equation (5) represents the "saddle point" approximation of the Jüttner distribution for $\Theta_n \ll 1$.[16] This assumption is consistent with the particle-in-cell simulation results, and, for many common scenarios, Eq. (5) effectively reduces to a cold Maxwellian distribution drifting at u_i.

If the phase offset $\Delta\phi$ between the laser electric field components is not precisely $\pi/2$, $\mathbf{f_L}$ also contains an oscillatory term that nonadiabatically accelerates "strongly" relativistic electrons.[13] These "hot" electrons are well-characterized by a Maxwell-Jüttner distribution,

$$f_{s_3}(\gamma) = \frac{n_h}{\Theta}\frac{\gamma^2\sqrt{1-\gamma^{-2}}}{K_2(1/\Theta)} e^{-\gamma/\Theta}, \tag{6}$$

where n_h is the hot electron density, γ is the Lorentz factor, $\Theta = T_h/(m_e c^2)$, T_h is the temperature and K_2 is the modified Bessel function of the second kind.

In the following sections, we seek to determine the parameters $\langle p_s^0\rangle$ of f_s that satisfy energy and momentum conservation between the ultraintense laser and plasma.

IV. RELATION BETWEEN THE PISTON AND HOLE PUNCHING VELOCITIES

In a time-averaged sense, ultraintense LPI at the critical density $n_{cr} = m_e\omega_L^2/(4\pi e^2)$ interface are characterized by the generation of a radiation pressure separation layer, comprised of electrons swept out by the laser fields, resulting in regions of charge compression and depletion. Ions are pulled along through the generation of a strong ambipolar force field, with the entire "laser piston" structure propagating into the bulk target at the piston velocity u_p. Particle mass density is conserved as the piston sweeps up and reflects background electrons and ions. From this, the relation between the piston velocity u_p and reflected ion velocity u_i can be obtained.

By integrating over Eq. (2) the continuity equation is obtained,

$$\frac{\partial\Gamma_s^\mu}{\partial x^\mu} = 0, \qquad \Gamma_s^\mu = \frac{n_s'}{m_s}P_s^\mu, \tag{7}$$

where n_s' is the Lorentz-invariant proper density of species s.[12] The fluid four-momentum $P_s^\mu = \gamma_s m_s c\,(1, \mathbf{V_s}/c)$ is defined as,

$$P_s^\mu = \frac{1}{n_s}\int p^\mu f_s\, \mathrm{d}p^k, \tag{8}$$

where the Lorentz factor $\gamma_s = (1 - \mathbf{V_s}\cdot\mathbf{V_s}/c^2)^{-1/2}$. The particle density n_s is given by,

$$n_s = \int f_s\, \mathrm{d}p^k. \tag{9}$$

We evaluate Eq. (7) by changing coordinates to the rest frame of the piston. Quantities in this frame are denoted using a superscript $(\prime p)$. For the laboratory frame velocity u, the appropriate Lorentz transformation is given by, $u^{(\prime p)} = (u - u_p)/(1 - u\cdot u_p/c^2)$. In this frame, the interaction is steady-state and longitudinal particle conservation may be expressed as

$$-Mn_i^{(\prime p)}u_p + Mn_i^{(\prime p)}u_i^{(\prime p)} = 0 \tag{10}$$

assuming ions are fully reflected by the laser piston. Here, u_p is the piston velocity, $n_i^{(\prime p)}$ is the ion density in the laser-plasma interface and $u_i^{(\prime p)}$ is the axial velocity of the reflected ions in the piston frame. Note that Eq. (10) represents particle conservation for both the hole punching electrons and ions, as $M = M_i + Zm_e$.

From Eq. (10), it follows that $u_i^{(\prime p)} = u_p$. Transforming back to the laboratory frame gives the hole punching ion axial velocity,

$$u_i = \frac{2u_p}{1 + (u_p/c)^2}, \tag{11}$$

consistent with Wilks *et al.*[1] in the nonrelativistic limit.

We now introduce the relativistic "hot" electron beam into this framework. This is possible due to the separation of velocity scales associated with the oscillatory and steady-state components of the nonlinear force. As was suggested by Ping *et al.*,[9] the plasma return current neutralizes the electron beam at a rate much faster than the piston velocity, i.e., $u_h/u_p \gg 1$ where $u_h \simeq c$ is the hot electron axial velocity. The interaction is thus steady-state on the piston timescale, such that the electron density as "seen" by the piston is unmodified. Particle number conservation for the hot electrons may then be written as

$$m_e n_e u_r + m_e n_h u_h = 0, \tag{12}$$

where $u_r = -(n_h/n_e)u_h$ is the return current velocity, i.e., a statement of the plasma neutralization of the hot electron beam current. The interplay between the laser light and the

plasma near the critical interface is illustrated schematically in Fig. 1.

In the framework of the usual two-temperature fit to the electron dN/dE energy spectrum,[8] the steady-state nonlinear force may be considered as corresponding to the low-energy component of the electron spectrum, and the oscillatory component as corresponding to the high-energy component. While the hot electrons may play a significant role energetically due to their relativistic γ-factor, in general, it is expected that n_h/n_e is small, as inspection of the electron energy spectrum from a typical experiment or simulation shows that the majority of the *number of electrons* in the system fall into the lower-energy component.

V. POYNTING THEOREM FOR ULTRAINTENSE LIGHT

Once the laser has excited populations s, their evolution is determined through conservation of phase volume given by Eq. (2). The parameters $\langle p_s^0 \rangle$ of f_s are determined by the four-divergence of the electromagnetic stress-energy tensor $T^{\mu\nu}$,

$$\frac{\partial T^{\mu\nu}}{\partial x^\nu} + \eta^{\mu k} \frac{\mathrm{d}p_k}{\mathrm{d}\tau} = 0, \tag{13}$$

where the characteristic is given in Eq. (3).

In this section, we will evaluate the four conservation laws implied by Eq. (13) in Euclidean space. This approach allows us to highlight effects related to the relativistic particle fluxes central to ultraintense laser-plasma interactions, while maintaining covariant notation in the following sections as appropriate.

Consider the electromagnetic energy density U_e in the box shown in Fig. 1. The Poynting theorem stipulates that

$$-\frac{\partial U_e}{\partial t} = \nabla \cdot \mathbf{S_e} + \sum_s \mathbf{J_s} \cdot \mathbf{E}, \tag{14}$$

where $\mathbf{S_e}$ is the electromagnetic Poynting flux and $\mathbf{J_s}$ is the electric current of species s.

As the light becomes ultraintense, the kinetic energy associated with the relativistic particle flux becomes significant. To elucidate this effect, the term in Eq. (14) corresponding to the work done against the Lorentz force can be written as

$$\sum_s \mathbf{J_s} \cdot \mathbf{E} = \frac{\partial U_m}{\partial t} + \nabla \cdot \mathbf{S_m}, \tag{15}$$

where U_m is the "mechanical" energy density in the box. $\mathbf{S_m}$ is the mechanical Poynting vector corresponding to a sum over the particle energy flux density,

$$\mathbf{S_m} = \sum_s (\gamma_s - 1) \mathbf{V_s} \, m_s n_s c^2. \tag{16}$$

A form of Poynting's theorem useful to ultraintense laser interactions is obtained by substituting Eqs. (15) and (16) into Eq. (14),

$$\frac{\partial U}{\partial t} + \nabla \cdot (\mathbf{S_e} + \mathbf{S_m}) = 0, \tag{17}$$

where $U = U_e + U_m$ is the total energy density in the region. Equation (17) states that in a steady-state interaction for the region in Fig. 1, the sink in the electromagnetic Poynting flux must be balanced by a source of kinetic particle flux.

It is straight forward to derive an analogous conservation law for the vector momentum flux density,

$$\frac{\partial \mathfrak{p}}{\partial t} + \nabla \cdot (\mathfrak{P}_\mathbf{e} + \mathfrak{P}_\mathbf{m}) = 0, \tag{18}$$

where $\mathfrak{P}_\mathbf{e}$ and $\mathfrak{P}_\mathbf{m}$ are second rank tensors describing the flow of electromagnetic and mechanical momentum flux, and $\mathfrak{p}$ is the total momentum density in the box in Fig. 1.

We conclude this section by commenting on the dynamical nature of the laser-plasma interface. The fact the interface is in motion in the laboratory frame plays an important role in satisfying Eqs. (17) and (18). In general, an electromagnetic flux through a surface moving at velocity u_p becomes,

$$\mathbf{S_e} \rightarrow \left(1 - \frac{u_p}{c}\right) \mathbf{S_e}, \quad \mathfrak{P}_\mathbf{e} \rightarrow \left(1 - \frac{u_p}{c}\right) \mathfrak{P}_\mathbf{e}. \tag{19}$$

In Sec. VI, these conservation laws will be applied to determine the properties of f_s for the exchange-mediating particle populations in Eq. (1).

VI. FULLY RELATIVISTIC MODEL OF ULTRAINTENSE LASER LIGHT ABSORPTION

Using the tools in the preceding sections, we now develop a model of ultraintense laser light absorption by an overdense plasma. For the first time, both hot electrons and hole punching particles are described relativistically and exchange both energy and momentum with the laser.

We consider the *steady-state* laser-plasma interaction *at the coupling stage* in the *laboratory frame*. The ensemble average momentum and kinetic energy for each population excited by the laser are given by

$$\langle \mathbf{p_s} \rangle = P_s^k, \tag{20}$$

$$\langle \mathcal{E}_s \rangle = P_s^0 \, c - m_s c^2. \tag{21}$$

The brackets are employed to emphasize that Eqs. (20) and (21) represent ensemble average quantities.

Over time interval d t, the total energy and momentum coupled by the laser into the particles in Eq. (1) is simply,

$$\begin{aligned} \mathrm{d}\mathcal{E}_s &= N_s \, \mathrm{d}\langle \mathcal{E}_s \rangle + \langle \mathcal{E}_s \rangle \, \mathrm{d}N_s, \\ \mathrm{d}\mathbf{p_s} &= N_s \, \mathrm{d}\langle \mathbf{p_s} \rangle + \langle \mathbf{p_s} \rangle \, \mathrm{d}N_s, \end{aligned} \tag{22}$$

where N_s is the particle number and the steady-state assumption implies that $\mathrm{d}\langle \mathcal{E}_s \rangle$ and $\mathrm{d}\langle \mathbf{p_s} \rangle$ are zero.

The number of ions accelerated by the laser piston over d t is,

$$\mathrm{d}N_{s_1} = n_i u_p \, \mathrm{d}A \, \mathrm{d}t, \tag{23}$$

where $dA = 2\pi r dr$ for a uniform laser spot of radius r. As in previous sections, n_i is the ion density in the interface and u_p is the piston velocity. By Eq. (10), the number of hole punching electrons excited over dt is $dN_{s2} = [Z \times$ Eq. (23)]. In this analysis, we consider a "slab" density profile, i.e., $n = n_0$, which is a sufficiently general representation of the overdense LP interaction. A slowly changing heterogeneous plasma profile, e.g., an exponential scalelength density profile $n(\mathbf{x})$, can be accounted for through the straight-forward substitution$n_0 \rightarrow n(\mathbf{x})$. This is due to the fact that each surface along a curvilinear plasma profile may be considered to be "slab" differentially.[7] The role of large-scale underdense plasma regions is commented on briefly at the end of this section and in Sec. VII.

The ensemble average particle energy and momentum can be related to the laser-plasma kinematic exchange using Eqs. (5), (16)–(18), and (20)–(23). The 1-D momentum and energy flux associated with the hole punching particles can be calculated as,

$$\begin{aligned} \mathcal{P}_{s_n} &= \frac{dp_n}{dA\, dt} = \langle p_n \rangle u_p n_n, \\ \mathcal{F}_{s_n} &= \frac{d\mathcal{E}_n}{dA\, dt} = \langle \mathcal{E}_n \rangle u_p n_n, \quad n \in \{1,2\}, \end{aligned} \tag{24}$$

where $\mathcal{P}_{s_n}$ ($\mathcal{F}_{s_n}$) is the momentum (energy) flux. As in the previous sections, $n_{s_1} = n_i, n_{s_2} = Zn_i$.

On the other hand, the number of hot electrons dN_{s_3} excited by the oscillatory component of the laser over dt is not directly related to the piston dynamics. As noted in Eq. (12), particle number is conserved in the interaction with the plasma return current on a timescale fast compared to u_p. From Eqs. (6), (20) and (21), we can assume that the hot electron momentum and energy flux densities are given by

$$\mathcal{P}_{s_3} = \gamma_h n_h m_e u_h^2, \qquad \mathcal{F}_{s_3} = (\gamma_h - 1) u_h n_h m_e c^2, \tag{25}$$

where $u_h \simeq c$ is the hot electron axial velocity. In contrast to n_{s_1} and n_{s_2}, n_h is an *ansatz* for the hot electron density. We assume the hot electron beam is directed longitudinally and symmetric about the beam axis. Thus, the transverse momentum terms related to Eq. (25) cancel one another on the scale c/ω_{pe}. A consequence of Eqs. (17) and (18) is that effects downstream of the interaction region are abstracted from the analysis, e.g., as the background plasma absorbs momentum and scatters the relativistic beam. In taking the kinematic form of Eq. (25), no assumptions are made with respect to the hot electron dynamical motion.[5] γ_h corresponds to the ensemble average hot electron Lorentz factor; brackets have been omitted for simplicity of notation.

Equations (24) and (25) constitute the mechanical Poynting flux $\mathbf{S_m}$ in Eq. (17). Integrating over the volume of the box in Fig. 1 and invoking the Divergence theorem gives,

$$\frac{1}{A_b} \int\int \mathbf{S_m} \cdot d\mathbf{A_b} = -\sum_s \mathcal{F}_s, \tag{26}$$

as the particle flux leaves the region on the right side. Here, $\mathbf{A_b}$ is the area of the surface bounding the box, with vector direction normal to the surface.

Noting Eq. (19), the laser Poynting flux in Eq. (17) in integral form can be written as

$$\frac{1}{A_b} \int\int \mathbf{S_e} \cdot d\mathbf{A_b} = \left(1 - \frac{u_p}{c}\right)(1 - \mathcal{R}) I_L, \tag{27}$$

where I_L is the laser intensity reaching the overdense surface and $\mathcal{R}$ is the fraction of reflected irradiance. Using Eqs. (26) and (27), the fully relativistic energy flux conservation equation can be expressed as

$$(1 - \mathcal{R})(1 - \beta_p) I_L = (\gamma_h - 1) m_e n_h c^3 + (\gamma_i - 1) M n_i \beta_p c^3, \tag{28}$$

where $M = M_i + Zm_e$ as in the preceding sections, $\beta_p = u_p/c$ is the dimensionless piston velocity, u_i is given by Eq. (11) and $\gamma_i = (1 + \beta_p^2)/(1 - \beta_p^2)$. The first term on the right-hand side of Eq. (28) represents coupling of the ultraintense laser light into the oscillatory mode of the nonlinear force, and the second term corresponds to coupling into the steady-state mode, the kinetic manifestation of which is the bulk electrons and ions reflected from the piston. The fast electron current neutralization described by $[(e/m_e) \times$ Eq. (12)] represents a collective response of the plasma to the beam. As noted above, the energy driving the return current is extracted from the beam itself and thus does not factor into the coupling equations.

Similarly, momentum flux conservation from Eq. (18) can be expressed as

$$(1 + \mathcal{R})(1 - \beta_p) \frac{I_L}{c} = \gamma_h m_e n_h c^2 + \gamma_i \beta_p M n_i u_i c, \tag{29}$$

where Eqs. (24) and (25) have been used.

Full reflection of background particles implies that the radiation pressure layer remains essentially depleted of electrons. It is thus clear that the fast electrons must be primarily generated at supercritical densities and may be shielded by the bulk target electrons from the full ponderomotive potential. As such, it is emphasized that γ_h does not *a priori* follow the ponderomotive scaling,[1] i.e., $\gamma_h \neq (1 + a_0^2)^{1/2}$, but rather may be self-consistently determined through Eqs. (28) and (29).

Employing the relation $2I_L/c = m_e n_{cr} a_0^2 c^2$, Eqs. (28) and (29) may be reformulated as,

$$(1 - \beta_p)(1 + \mathcal{R}) = \frac{\gamma_h}{\beta_0^2} \frac{m_e}{M} \frac{n_h}{n_i} + \frac{1}{\beta_0^2} \frac{2\beta_p^2}{1 - \beta_p^2}, \tag{30}$$

$$(1 - \beta_p)(1 - \mathcal{R}) = \frac{(\gamma_h - 1)}{\beta_0^2} \frac{m_e}{M} \frac{n_h}{n_i} + \frac{\beta_p}{\beta_0^2} \left(\frac{1 + \beta_p^2}{1 - \beta_p^2} - 1 \right), \tag{31}$$

where β_0 is the dimensionless shock velocity scale,

$$\beta_0 = \left(\frac{I_L}{n_i M_i c^3} \right)^{1/2} = \left(\frac{Z m_e}{2 M_i} \frac{n_{cr}}{n_e} \right)^{1/2} a_0. \tag{32}$$

As β_0 becomes closer to unity, it no longer closely approximates the actual piston velocity β_p. For simplicity of notation, we adopt the convention that linear light with

normalized potential a_0 has identical energy density to circular light of $a_0/\sqrt{2}$.

$\{\gamma_h, \beta_p\}$ parameterize f_s and thus determine the LP equilibrium condition. Problematically, however, Eqs. (30) and (31) make evident the additional degree of freedom associated with the hot electrons, n_h. We treat this by defining,

$$\bar{\rho}_h \equiv \frac{\rho_h}{\sum \rho} = \frac{Zm_e}{M}\frac{n_h}{n_e}, \tag{33}$$

where $\bar{\rho}_h$ represents the *relative mass density* in the interaction region coupled into the oscillatory mode. While the electrons may play a significant role energetically due to the relativistic γ-factor, Eq. (33) shows that $\bar{\rho}_h \ll 1$, as the maximum value of $\bar{\rho}_h \sim Zm_e/M$ as $n_h/n_e \sim 1$.

Having identified the small parameter $\bar{\rho}_h$, we may reduce the dimensionality of the problem by taking a series expansion of the solutions to Eqs. (30) and (31). To zeroth order in $\bar{\rho}_h$, we calculate,

$$\beta_p = \beta_0 \left(\frac{\mathcal{R}}{1+\mathcal{R}\beta_0^2}\right)^{1/2}. \tag{34}$$

Equation (34) is independent of $\bar{\rho}_h$, showing that the interplay between the piston velocity β_p and light coupled into the oscillatory mode is indirect, occurring only as the fast electron absorption increases the total light absorbed by the plasma. Equation (34) also predicts a decrease in piston velocity as total absorption increases, with $\beta_p \to 0$ as $\mathcal{R} \to 0$. This limit is related to the cases described by Haines *et al.*[5] and Ping *et al.*[9]

Equation (34) represents the fully relativistic hole punching velocity, taking into account both oscillatory hot electron generation and steady-state acceleration of background particles by the laser piston. This expression is valid for overdense laser-plasma interactions, while background ions are fully reflected by the laser light, independent of the laser polarization and fraction of reflected light $\mathcal{R}$. The parametric instabilities associated with relativistic light interacting with an underdense plasma represent additional vectors through which the light may couple to the plasma, and have been shown to lead to the formation of a supraponderomotive tail in the electron spectrum.[17,18] In effect, this would increase the number of exchange-mediating populations in Eq. (1), e.g., Raman-scattering electrons.[8]

It bears noting here that results from well-established absorption models follow from Eq. (34) in specific limits. The piston velocity from Wilks *et al.*,[1] $\sqrt{(1+\mathcal{R})/2}\,\beta_0$, can be derived exactly from Eq. (29) in the limits that $n_h \to 0$ and $\beta_0 \ll 1$. This expression is close to our result for β_p in the nonrelativistic limit but diverges as $\beta_p \gtrsim 0.1$. It is straight-forward to show that the relativistically correct piston velocity for 100% conversion efficiency into ions as found by Naumova *et al.*,[7] $u_p/c = \beta_0/(1+\beta_0)$, represents a contour along the surface defined by Eq. (34). Indeed, this result follows exactly from our Eqs. (28) and (29) in the limit $n_h \to 0$. It should also be noted that Eq. (34) reduces in the nonrelativistic ion limit to $\sqrt{\mathcal{R}}\,\beta_0$, equivalent to the expression found in Ref. 9 for linearly-polarized light, despite quite distinct assumptions in the underlying model.

From Eqs. (30), (31), and (34), we find that the solution for γ_h contains two terms to zeroth order in $\bar{\rho}_h$,

$$\gamma_h = \frac{(1-\mathcal{R})\sqrt{\beta_0^2\mathcal{R}+1} - \beta_0\sqrt{\mathcal{R}}(1+\mathcal{R})}{\sqrt{\beta_0^2\mathcal{R}+1}\,\beta_0^{-2}}\,\bar{\rho}_h^{-1} + O(1). \tag{35}$$

The $O(1)$ term is a polynomial in β_0 and $\mathcal{R}$. γ_h is a moment of f_{s3} and thus represents a robust measure of the ensemble-average hot electron energy. Fig. 2 shows the contours of the $O(1)$ term. Fig. 3 depicts the solutions $\{\gamma_h, \beta_p\}$ from Eqs. (34) and (35). The ensemble average hot electron energy γ_h scales as $\sim\bar{\rho}_h^{-1}$, while from Eq. (28) the total energy coupled into the oscillatory mode $\sim\gamma_h\,\bar{\rho}_h$ is independent of the parameter. This relationship is borne out by particle-in-cell simulation results and will be discussed in more detail in Secs. VII and VII.

With the piston velocity β_p in Eq. (34) and the ensemble average hot electron energy γ_h in Eq. (35), the distribution function moments $\langle p_s^0 \rangle$ of f_s in Eq. (1) are fully characterized. Together with Eq. (11) relating u_i to the piston velocity, these equations satisfy energy and momentum conservation between an ultraintense laser and overdense plasma.

VII. CONVERSION EFFICIENCY INTO HOT ELECTRONS AND HOLE PUNCHING IONS

Finally, let us consider the conversion efficiency of laser light into populations listed in Eq. (1).

From Eqs. (31) and (34), we can calculate the conversion efficiency into hot electrons,

$$f_a^h = (\gamma_h - 1)\,\bar{\rho}_h \frac{\beta_0^{-2}}{1 - \beta_0\sqrt{\dfrac{\mathcal{R}}{\beta_0^2\mathcal{R}+1}}}. \tag{36}$$

Using Eq. (35), this expression can be expanded as,

$$f_a^h = \frac{(1-\mathcal{R})\sqrt{\beta_0^2\mathcal{R}+1} - (1+\mathcal{R})\beta_0\sqrt{\mathcal{R}}}{\sqrt{\beta_0^2\mathcal{R}+1} - \beta_0\sqrt{\mathcal{R}}} + O\left(\frac{\bar{\rho}_h}{\beta_0^2}\right). \tag{37}$$

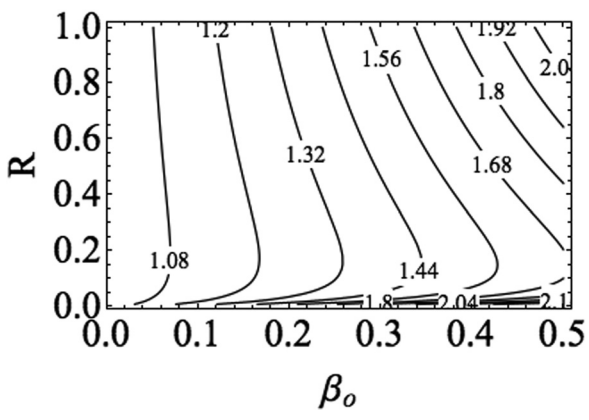

FIG. 2. Contours of the $O(1)$ term from Eq. (35).

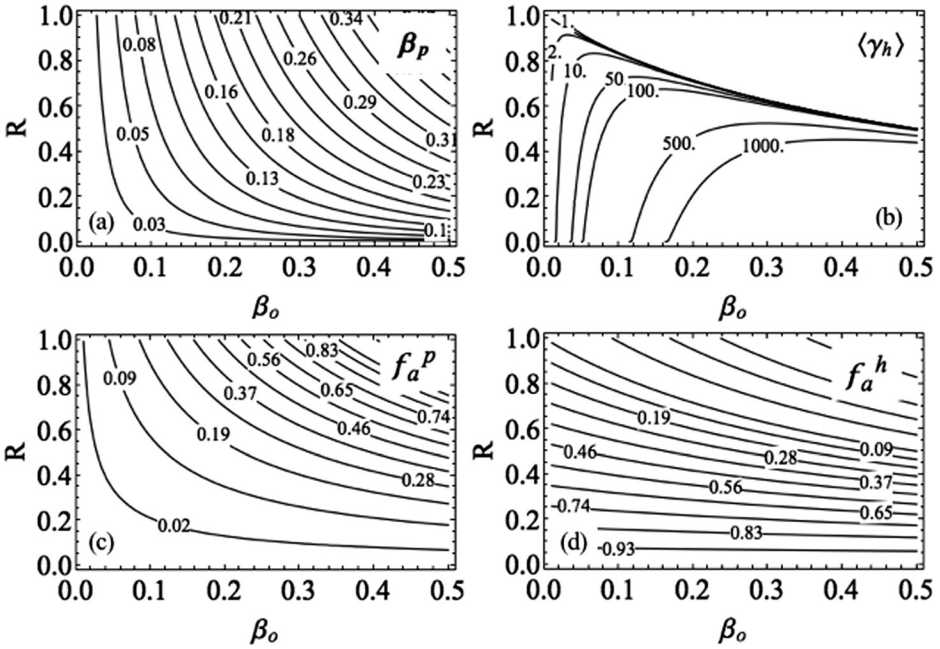

FIG. 3. (a) and (b) Analytic solutions satisfying energy and momentum conservation with the laser, $\{\gamma_h, \beta_p\}$. (c) and (d) Contours of the laser conversion efficiencies into each absorption mode.

Equation (37) illustrates the key result that the total energy coupled into electrons f_a^h depends only on β_0 and $\mathcal{R}$, while $\bar{\rho}_h/\beta_0^2 \ll 1$.

For the laser conversion efficiency into hole punching ions, f_a^p, we have,

$$f_a^p = \frac{2\beta_0\mathcal{R}^{3/2}}{\sqrt{\beta_0^2\mathcal{R}+1}-\beta_0\sqrt{\mathcal{R}}}. \tag{38}$$

As for f_a^h, we observe that the conversion efficiency into hole punching ions is robust to the hot electron mass density $\bar{\rho}_h$. The conversion efficiencies from Eqs. (37) and (38) highlight the nonlinear dependency of the coupling on the shock velocity scale β_0 and the total light absorption $1-\mathcal{R}$. The solutions for the conversion efficiencies are depicted in Fig. 3.

In concluding this section, we briefly comment on the boundary conditions associated with the total light absorption. For the case of circular polarization, corresponding to the limit $n_h \to 0$, the upper limit to the reflection was calculated in Ref. 7 to be $\mathcal{R} = 1/(1+2\beta_0)$. Strictly speaking, it would be incorrect to impose this limit on the general system, in which both the hot electron and hole punching absorption modes are accounted for. This will be investigated in future work, as there are additional complexities associated with deriving the limit on $\mathcal{R}$ in the general case.

In the following section, we will compare the predictions of Eqs. (37) and (38) to particle-in-cell simulations.

VIII. PARTICLE-IN-CELL SIMULATIONS AND POSSIBLE ASTROPHYSICAL APPLICATIONS

To test the predictions of the analytic model, we have performed PIC simulations using the hybrid LSP code.[19] The code is configured to solve the discretized Maxwell's equations and Lorentz force equation implicitly, with no time biasing to avoid numerical damping of light waves. The timestep is determined by the Courant condition multiplied by a factor of 0.1. Electrons and ions are fully kinetic and are represented using 500 particles/cell/species. We have modified the LSP source code to implement a "kinetic-to-kinetic" particle migration feature. This allows us to effectively distinguish, label and track electrons which interact with the laser and exceed a kinetic energy threshold from the cold background.

Simulations are one-dimensional Cartesian geometry with uniform spatial resolution $(\Delta x)^{-1} = 16\,\text{cells}/\mu\text{m}$ resolving the relativistic collisionless skin depth. Laser light enters the box at the left $x=0$ boundary and is incident upon an overdense $Z/A=1$ plasma slab at $x=5\,\mu$m. The slab density ramps to peak density $n_0 = n_e = Zn_i$ over $0.06\,\mu$m and has a $290\,\mu$m spatial extent, followed by $5\,\mu$m of vacuum ahead of the right boundary; the box is effectively infinite to prevent electron refluxing. The laser pulse has $1\,\mu$m wavelength and rises over 3 optical cycles to a flat-top profile with 500–700 fs duration. The plasma density n_0 and normalized laser amplitude a_0 are varied across simulations.

We exploit optical polarization to investigate laser coupling to the populations in Eq. (1). Starting from circular light, by "detuning" the phase offset between the laser electric field components we can precisely examine the system as increasing energy is coupled into the oscillatory mode, as $|\langle\mathbf{f_L}\rangle - \mathbf{f_L}| > 0$. Our method is as follows: two lasers are injected through the $x=0$ boundary, each linearly polarized in the opposite plane with normalized intensity $a_0/\sqrt{2}$. From this setup, precise control over the oscillatory electron energy is possible by tuning the relative offset between the phases of the two waves, $\Delta\phi$ [rad]. In this notation, $\Delta\phi = \pi/2$ corresponds to circular light and $\Delta\phi = 0$ corresponds to linear light, with the total amplitude of the light equal to a_0 for arbitrary $\Delta\phi$. We have checked that the $\Delta\phi = 0$ simulations agree closely with simulations performed using a single linearly-polarized laser. This approach has an important experimental analog, as maintaining ideal polarization phases is challenging under realistic conditions.

Fig. 4 compares analytic predictions to simulation results for various $a_0, n_0, \Delta\phi$ configurations. (a)–(d) show the simulation results for the energy coupled into the oscillatory and steady-state absorption modes. Predictions from the model for f_a^h and f_a^p from Eqs. (37) and (38) are overlaid on the figures, calculated using reflection data from the simulations at 60 fs intervals. The absorption model is seen to agree with the simulation data to within one percent.

As illustrated in the legend, the cumulative particle energy is normalized to the total field energy injected into the simulation for an equivalent "empty" run with no plasma. The simulation instantaneous particle energy flux is normalized to the attenuated injected energy flux density from the laser as noted in Eq. (29). We find that the proper normalization coefficients,

$$C_0 = (1-\beta_p) I_L, \qquad C_1 = \int I_L \, dA \, dt, \tag{39}$$

are essential so that measurements of the instantaneous coupling agree with measurements of the cumulative energy coupling, confirming Eq. (19). With this approach, we have checked that the full time-integrated photon energy passing through the simulation boundaries agrees with the total and instantaneous energy absorbed into particles.

We note that care must be taken in measuring the instantaneous reflection using light passing through the simulation boundaries, as the energy flux associated with the reflected photons undergoes both doppler red-shifting and dispersion over time, due to the additional distance $dx = 2u_p dt$ traveled. Because I_L corresponds to the laser light reaching the overdense target surface, as noted in Eq. (27), care must also be taken in scenarios with large-scale underdense plasma regions.

Fig. 4(e) shows the corresponding piston velocity β_p from the simulations and analytic model. The velocity from the simulation is measured using two methods: first, the location of the interface defined by $n_i/n_0 = 1$ is tracked at 10fs intervals. The solid curves represent the derivative of this "front" or piston location over time. Second, we measure the doppler-shifting[8,9] in the frequency of the $1\omega_L$ light in the E_z transverse electric field passing through the simulation boundary. The relativistic piston velocity β_p is related to the frequency shift through $\Delta f/f_0 = 1 - (1-\beta_p)/(1+\beta_p)$. The diamond markers represent the Fourier transformed simulation data at 100 fs intervals. The analytic model predictions are seen to be within one percent of the simulation data across laser intensities and polarizations. Fig. 4(b) depicts the $a_0 = 20\sqrt{2}, n_0/n_{cr} = 20, \Delta\phi = \pi/2$ configuration, showing good agreement with results obtained in Ref. 14. Figs. 4(c) and 4(d) correspond to $a_0 = 100, n_0/n_{cr} = 30$, showing the steady-state interaction far below the relativistic critical density threshold.[10] The protons reflected from the piston in this simulation attain kinetic energy of ~100 MeV.

Figs. 4 and 5 illustrate the effects the laser polarization offset for the $a_0 = 100, n_0/n_{cr} = 30, Z/A = 1$ ($\beta_0 = 0.3$) plasma simulation. The electron and ion phase space from the simulation are depicted in Figs. 5(a), 5(b), and 5(d) and 5(e). The hot electron energy spectra across $\Delta\phi$ are depicted in Fig. 5(c). In the $\Delta\phi = 0.92$ simulation, the laser piston is observed to reflect background ions effectively even as 10% more energy is coupled into the oscillatory mode electrons, relative to the $\Delta\phi = \pi/2$ simulation. Fig. 5(e) compares the model predictions to the simulation results across polarizations. For the $\Delta\phi = \pi/2, 0.95, 0.92$ simulations, the conversion efficiencies are in agreement to <2%. As the polarization tends further towards linear, simulation results show a jump in the total energy absorbed by the plasma. This is due to the fact that the laser piston no longer fully reflects ions, allowing electrons to fall through the piston potential. Consistent with the assumptions underlying the model, accuracy falls beyond this point as additional effects such as shock acceleration of ions modify the partitioning of energy coupled into the plasma. The dynamics of these effects, recently reported on in detail,[20] fall outside the scope of this paper.

Laser coupling into the oscillatory absorption mode is illustrated in Fig. 6 for the $\beta_0 = 0.3, \Delta\phi = 0.92$ simulation, corresponding to $a_0 = 100$, $n_e/n_{cr} = 30$, $Z/A = 1$. (a)

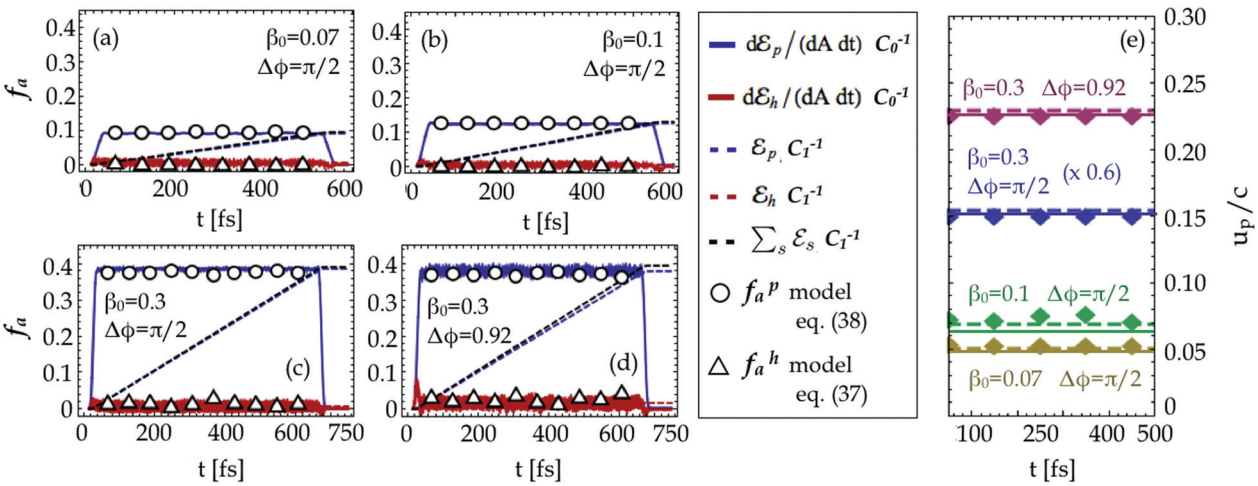

FIG. 4. Comparison to particle-in-cell simulations. (a)–(d) Light coupling into the steady-state and oscillatory ponderomotive absorption modes. (e) Piston velocity β_p from the simulations and analytic model. Solid lines correspond to dx_p/dt and diamond markers correspond to the velocity inferred from 1ω doppler shift measurements from the simulations (see text). Dashed lines represent the analytic β_p from Eq. (34).

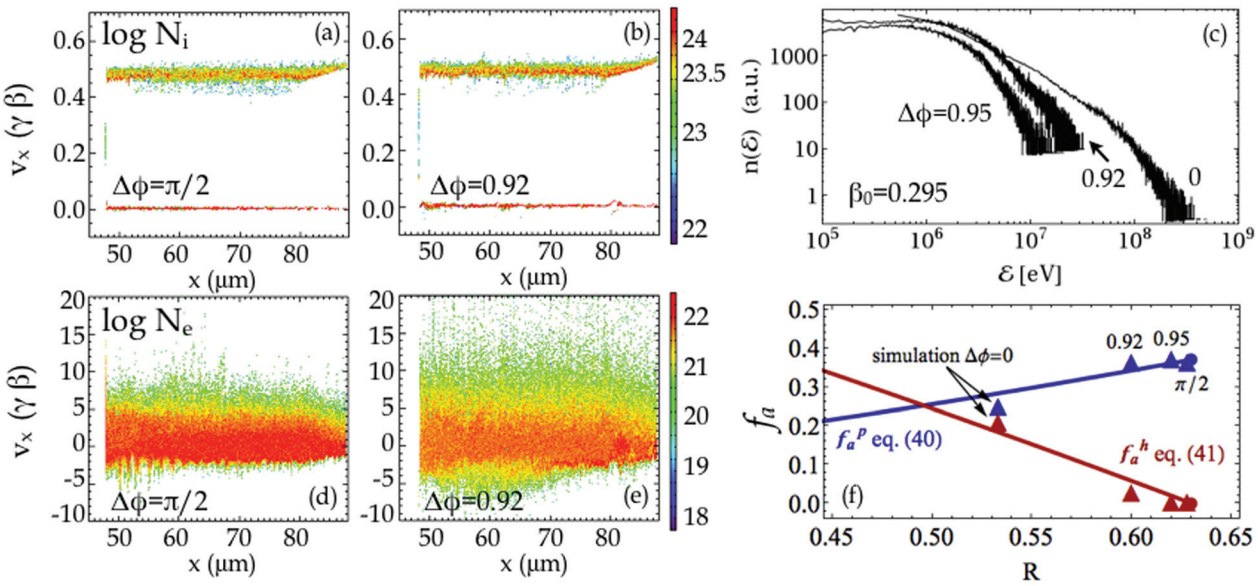

FIG. 5. Simulation and analytics for the $\beta_0 = 0.3$ laser-plasma interaction. (a) and (b) Ion and (d) and (e) electron phase space from simulations. (c) Hot electron spectra from simulations (relative $n(\mathcal{E})$ not to scale). (f) Comparison of laser absorption analytic predictions and simulation results.

depicts the density of exchange mediating electrons (red) and of ions (black) at two times, with the arrows indicating the dynamical position of the laser-plasma interface. The density of electrons coupled into the oscillatory mode, n_h, is calculated in the simulation as the subset of exchange-mediating electrons passing through the $x = 100\,\mu$m plane as shown in (b). The associated relative mass density $\bar{\rho}_h \ll 1$ given by Eq. (33) is labeled on the right axis. (d) depicts the ensemble average Lorentz factors for the exchange-mediating electrons and for the hot electrons. The conversion efficiency into hot electrons is examined in detail in Fig. 6(c). Three quantities are depicted: first, the analytic model for f_a^h from Eq. (37). The dashed black curve depicts this using the parameters β_0 and the average reflection coefficient $\mathcal{R} = 0.61$ from Fig. 4. Second, the hot electron energy flux density $d\mathcal{E}_h/(dA\,dt)$ is self-consistently calculated through a diagnostic in the simulation. The red curve shows this quantity normalized to Eq. (39) using the constant laser intensity I_L. Third, the expression for f_a^h calculated using the simulation γ_h from (d) and $\bar{\rho}_h$ from (b). These quantities are constrained in a well-defined fashion, according to Eqs. (30) and (31). The solid black curve depicts f_a^h from Eq. (36) calculated using γ_h and $\bar{\rho}_h$, confirming this relationship. In sum, Figs. 4–6 demonstrate excellent agreement between the analytic model and simulation results.

The results presented in this paper for the deposition of laser energy into hole punching ion and hot electron components are germane to topical astrophysical sources. Notably, such conversion efficiencies are core unknowns in the study of astrophysical jets in gamma-ray bursts (GRBs) and blazars. Most GRBs are thought to emanate from powerful explosions of hypermassive stars located in distant galaxies in the early universe, at redshifts of around $z = 1$ or larger.[21,22] Their enormous energy release drives a collimated, ultra-relativistic outflow (i.e., jet) with bulk Lorentz factors Γ in excess of several hundred.[23,24] Blazars are also extragalactic jet sources, but generally nearer by and less luminous than GRBs, and with inferences of less extreme bulk motions ($\Gamma \sim 3 - 50$). They emanate from the environs of persistent supermassive black holes. There is a growing enthusiasm among astrophysicists for the paradigm that Poynting flux-dominated outflows in gamma-ray bursts (e.g., Refs. 25 and 26) and blazars (e.g., Refs. 27 and 28, and references therein) drive their energization, precipitating radiative dissipation at large distances from their central engines. Understanding the efficiency of conversion of direct

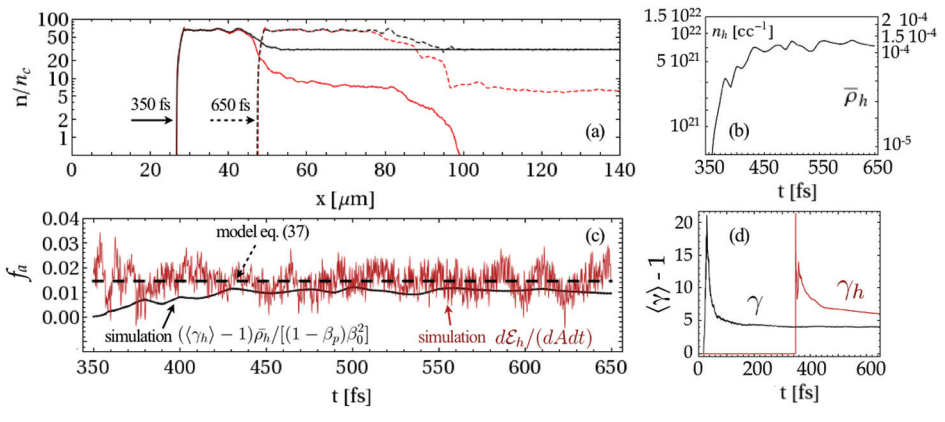

FIG. 6. Coupling to the oscillatory component of the laser ponderomotive force for the $\beta_0 = 0.3$, $\Delta\phi = 0.92$ simulation. (a) Number density of exchange-mediating electrons (red) and of ions (black). Arrows indicate the position of the laser-plasma interface. (b) Hot electron density n_h and $\bar{\rho}_h$. (c) Comparison of hot electron absorption from the simulation to the analytic model. (d) Ensemble average Lorentz factors (see text).

electromagnetic energy to plasma kinetic and thermal energies is therefore an extremely desirable advance. Laser-driven plasma interaction and associated kinetics can therefore provide crucial insights into these astrophysical phenomena, especially in light of the fact that the electromagnetic energy densities excited by petawatt class lasers are not widely disparate from those in blazer and GRB jets. This study and its results on laser light absorption are an important step in this direction. Formulating simple equations such as Eq. (37) to describe the ultimate kinematic apportionment of laser energy into hot electrons provides a first guide to how efficiently we think gamma-ray bursts and blazars can radiate if their outflows are mediated mostly by Poynting flux at early epochs in their expansion. Establishing a firmer relationship between the two regimes will be the subject of future work.

IX. CONCLUSION

In conclusion, we have developed a more comprehensive model of ultraintense laser absorption, allowing the light to couple into both the hole punching and hot electron absorption modes in an energetically significant fashion for the first time. The fully relativistic model has been derived for arbitrary overdense interaction densities and is insensitive to laser polarization assuming that bulk ions are swept up and fully reflected by the laser piston.

Using this framework, we have obtained solutions for the particle distribution function moments that simultaneously satisfy energy and momentum conservation, i.e., the relativistically correct piston velocity including the hot electrons, and the hot electron Lorentz factor. For the first time, analytic expressions for the conversion efficiencies into hole punching ions and into hot electrons have been derived. The model establishes robust kinematic constraints on the relationships between the total absorption and the fundamental laser and plasma quantities and recovers well-established results (e.g., for the piston velocity) in specific limits. Close agreement between the analytic model and particle-in-cell simulations has been demonstrated, justifying the assumptions underlying the kinematic approach. These results open the door to addressing a number of interesting ultraintense laser plasma applications in the future.

ACKNOWLEDGMENTS

M.L. is grateful to S. Libby for stimulating conversations and to he and L. Divol for their encouragement of continued research into basic laser plasmas. M.L. also thanks W. Rozmus for advice on lexical aspects and F. Fiuza and A. Link for useful discussions.

This work was performed under the auspices of the U.S. Department of Energy by Lawrence Livermore National Laboratory under Contract No. DE-AC52-07NA27344.

[1]S. C. Wilks, W. L. Kruer, M. Tabak, and A. B. Langdon, "Absorption of ultra-intense laser pulses," Phys. Rev. Lett. **69**(9), 1383–1386 (1992).
[2]V. Malka, J. Faure, Y. A. Gauduel, E. Lefebvre, A. Rousse, and K. Ta Phuoc, "Principles and applications of compact laser-plasma accelerators," Nature Phys. **4**(6), 447–453 (2008).
[3]M. Tabak, J. Hammer, M. E. Glinsky, W. L. Kruer, S. C. Wilks, J. Woodworth, E. Michael Campbell, M. D. Perry, and R. J. Mason, "Ignition and high gain with ultrapowerful lasers," Phys. Plasmas **1**, 1626–1634 (1994).
[4]S. V. Bulanov, T. Zh. Esirkepov, V. S. Khoroshkov, A. V. Kuznetsov, and F. Pegoraro, "Oncological hadrontherapy with laser ion accelerators," Phys. Lett. A **299**(23), 240–247 (2002).
[5]M. Haines, M. Wei, F. Beg, and R. Stephens, "Hot-electron temperature and laser-light absorption in fast ignition," Phys. Rev. Lett. **102**(4), 045008 (2009).
[6]H. Chen, S. C. Wilks, J. Bonlie, E. Liang, J. Myatt, D. F. Price, D. D. Meyerhofer, and P. Beiersdorfer, "Relativistic Positron creation using ultraintense short pulse lasers," Phys. Rev. Lett. **102**(10), 105001 (2009).
[7]N. Naumova, T. Schlegel, V. Tikhonchuk, C. Labaune, I. Sokolov, and G. Mourou, "Hole boring in a DT pellet and fast-ion ignition with ultraintense laser pulses," Phys. Rev. Lett. **102**(2), 025002 (2009).
[8]S. C. Wilks and W. L. Kruer, "Absorption of ultrashort, ultra-intense laser light by solids and overdense plasmas," IEEE J. Quantum Electron. **33**(11), 1954–1968 (1997).
[9]Y. Ping, A. Kemp, L. Divol, M. Key, P. Patel, K. Akli, F. Beg, S. Chawla, C. Chen, R. Freeman, D. Hey, D. Higginson, L. Jarrott, G. Kemp, A. Link, H. McLean, H. Sawada, R. Stephens, D. Turnbull, B. Westover, and S. Wilks, "Dynamics of relativistic laser-plasma Interaction on solid targets," Phys. Rev. Lett. **109**(14), 145006 (2012).
[10]F. Cattani, A. Kim, D. Anderson, and M. Lisak, "Threshold of induced transparency in the relativistic interaction of an electromagnetic wave with overdense plasmas," Phys. Rev. E **62**(1 Pt B), 1234–1237 (2000).
[11]H. Ruhl and P. Mulser, "Relativistic Vlasov simulation of intense fs laser pulse-matter interaction," Phys. Lett. A **205**, 388–392 (1995).
[12]R. D. Hazeltine and S. M. Mahajan, "Generalization of collisional fluid theory to long mean-free-path and relativistic motion," Phys. Plasmas **9**(8), 3341 (2002).
[13]W. L. Kruer and K. Estabrook, "J-B heating by very intense laser light," Phys. Fluids **28**(1), 430 (1985).
[14]T. Schlegel, N. Naumova, V. T. Tikhonchuk, C. Labaune, I. V. Sokolov, and G. Mourou, "Relativistic laser piston model: Ponderomotive ion acceleration in dense plasmas using ultraintense laser pulses," Phys. Plasmas **16**(8), 083103 (2009).
[15]A. P. L. Robinson, "Production of high energy protons with hole-boring radiation pressure acceleration," Phys. Plasmas **18**(5), 056701 (2011).
[16]L. A. Cottrill, A. B. Langdon, B. F. Lasinski, S. M. Lund, K. Molvig, M. Tabak, R. P. J. Town, and E. A. Williams, "Kinetic and collisional effects on the linear evolution of fast ignition relevant beam instabilities," Phys. Plasmas **15**(8), 082108 (2008).
[17]H. Daido, M. Nishiuchi, and A. S. Pirozhkov, "Review of laser-driven ion sources and their applications," Rep. Prog. Phys. **75**(5), 056401 (2012).
[18]A. Macchi, M. Borghesi, and M. Passoni, "Ion acceleration by superintense laser-plasma interaction," Rev. Mod. Phys. **85**(2), 751–793 (2013).
[19]D. R. Welch, D. V. Rose, R. E. Clark, T. C. Genoni, and T. P. Hughes, "Implementation of an non-iterative implicit electromagnetic field solver for dense plasma simulation," Comput. Phys. Commun. **164**(1–3), 183–188 (2004).
[20]F. Fiuza, A. Stockem, E. Boella, R. Fonseca, L. Silva, D. Haberberger, S. Tochitsky, C. Gong, W. Mori, and C. Joshi, "Laser-driven shock acceleration of monoenergetic ion beams," Phys. Rev. Lett. **109**(21), 215001 (2012).
[21]T. Piran, "Gamma-ray bursts and the fireball model," Phys. Rep. **314**(575) (1999).
[22]P. Mészáros, "Theories of gamma-ray bursts," Annu. Rev. Astron. Astrophys. **40**(137) (2002).
[23]M. G. Baring, "Temporal evolution of pair attenuation signatures in gamma-ray burst spectra," Astrophys. J. **650**(1004) (2006).
[24]A. A. Abdo *et al.*, "Fermi observations of high-energy gamma-ray emission from GRB 080916C," Science (New York) **323**(5922), 1688–1693 (2009).
[25]M. Lyutikov and R. D. Blandford, "Electromagnetic outflows and grbs," Astron. Soc. Pac. Conf. Ser. **312**(449) (2004).
[26]B. Zhang and A. Pe'er, "Evidence of an initially magnetically dominated outflow in grb 080916c," Astrophys. J. **700**(L65) (2009).
[27]T. Chiueh, M. C. Begelman, and Z.-Y. Li, "Electromagnetically driven relativistic jets—a class of self-similar solutions," Astrophys. J. **394**(459) (1992).
[28]G. M. Madejski, J.-P. Lasota, M. Sikora, and M. C. Begelman, "Are quasar jets dominated by poynting flux?," Astrophys. J. **625**(72) (2005).